

# Early-Matter-Like Dark Energy and the Cosmic Microwave Background

**R. Aurich and S. Lustig**

Institut für Theoretische Physik, Universität Ulm,  
Albert-Einstein-Allee 11, D-89069 Ulm, Germany

E-mail: [ralf.aurich@uni-ulm.de](mailto:ralf.aurich@uni-ulm.de), [sven.lustig@uni-ulm.de](mailto:sven.lustig@uni-ulm.de)

**Abstract.** Early-matter-like dark energy is defined as a dark energy component whose equation of state approaches that of cold dark matter (CDM) at early times. Such a component is an ingredient of unified dark matter (UDM) models, which unify the cold dark matter and the cosmological constant of the  $\Lambda$ CDM concordance model into a single dark fluid. Power series expansions in conformal time of the perturbations of the various components for a model with early-matter-like dark energy are provided. They allow the calculation of the cosmic microwave background (CMB) anisotropy from the primordial initial values of the perturbations. For a phenomenological UDM model, which agrees with the observations of the local Universe, the CMB anisotropy is computed and compared with the CMB data. It is found that a match to the CMB observations is possible if the so-called effective velocity of sound  $c_{\text{eff}}$  of the early-matter-like dark energy component is very close to zero. The modifications on the CMB temperature and polarization power spectra caused by varying the effective velocity of sound are studied.

**Keywords:** dark energy theory, CMBR theory

**ArXiv ePrint:** [1511.01691](https://arxiv.org/abs/1511.01691)

---

## Contents

<b>1</b>	<b>Introduction</b>	<b>1</b>
<b>2</b>	<b>The background model</b>	<b>3</b>
<b>3</b>	<b>Initial conditions and evolution of perturbations</b>	<b>4</b>
<b>4</b>	<b>CMB anisotropy for the arctan-UDM model</b>	<b>6</b>
<b>5</b>	<b>Summary</b>	<b>12</b>
<b>A</b>	<b>The power series of the potentials in conformal time</b>	<b>13</b>
<b>B</b>	<b>The generalised matter perturbations in terms of the potentials</b>	<b>15</b>
<b>C</b>	<b>The radiation perturbations in terms of the potentials</b>	<b>16</b>
<b>D</b>	<b>Isentropic initial condition</b>	<b>18</b>

---

## 1 Introduction

The  $\Lambda$ CDM concordance model successfully describes a variety of cosmological observations over many orders of length scales. However, only about five percent of the energy density of the universe can be ascribed to known particles of the standard model of elementary particle physics. The cold dark matter (CDM) and the dark energy components of the  $\Lambda$ CDM are introduced as two phenomenological components. There have been many attempts to naturally explain the dark energy in the framework of quintessence models, which explain it in terms of a scalar field governed by some potential. In contrast to the cosmological constant  $\Lambda$  of the  $\Lambda$ CDM model, which possesses a constant equation of state  $w = p/\varepsilon = -1$  with the pressure  $p$  and the energy density  $\varepsilon$ , quintessence scenarios allow a time-varying equation of state. Besides the equation of state, there are further degrees of freedom which characterise a possible phenomenological component as emphasised by [1], who introduced a generalised dark matter component defined by the effective velocity of sound  $c_{\text{eff}}$  (in the rest frame of the dark component) as well as a viscosity velocity  $c_{\text{vis}}$  which is related to the anisotropic stress. The usual cold dark matter is characterised by  $w = 0$ ,  $c_{\text{eff}}^2 = 0$  and  $c_{\text{vis}}^2 = 0$ , whereas for quintessence models, the parameters are  $c_{\text{eff}}^2 = 1$  and  $c_{\text{vis}}^2 = 0$  and  $w$  is restricted to  $-1 \leq w \leq 1$ .

Since the  $\Lambda$ CDM model requires two phenomenological components, one could ponder the issue whether a single phenomenological dark component might suffice. This component could have a time-varying equation of state  $w = w(t)$  and possibly non-standard values of  $c_{\text{eff}}^2$  and  $c_{\text{vis}}^2$ . In order to describe the accelerated expansion of the recent cosmos, one needs  $w(t) < -\frac{1}{3}$  for recent times. On the other hand, one has to ensure that the structure formation in the baryonic sector can evolve around the time of recombination as described in the framework of the  $\Lambda$ CDM model, which requires a significant dark matter component having  $w(t) = 0$  at early times. A phenomenological component with such a behaviour is called a unified dark matter (UDM) component.

The prototypical model for a UDM component is the Chaplygin gas which is originally considered in a cosmological context in [2], see also [3–7] for other early works and for the generalised Chaplygin gas having an equation of state  $p = -A/\varepsilon^\alpha$  with  $0 \leq \alpha \leq 1$ . In [8] it is shown that the parameter space of the generalised Chaplygin gas is confined to a very small domain with  $\alpha$  so close to zero that it is nearly identical to the  $\Lambda$ CDM model such that the motivation for the Chaplygin gas is undermined. For a discussion of the case  $\alpha > 1$ , where a causality problem arises, see [9]. A loophole for the restricted parameter space is provided by allowing the generation of entropy perturbations from adiabatic initial conditions. This corresponds to an effective speed of sound  $c_{\text{eff}}^2$  different from the adiabatic one [10]. In that paper, it is shown that a vanishing effective speed of sound  $c_{\text{eff}}^2$  suffices to reconcile the generalised Chaplygin gas with the matter power spectra  $P(k)$  for a large range of the parameter  $\alpha$ .

Also models with a non-canonical kinetic Lagrangian, so-called  $k$ -essence models, can provide a scenario for an UDM model as it is put forward in [11] where the simplest class of  $k$ -essence models with a constant potential term is considered. It is emphasised in [11] that a low sound speed in these models circumvents the difficulties of the Chaplygin gas discussed above since the integrated Sachs-Wolfe effect is then suppressed at large-angular scales [12, 13].

For a review discussing various unified dark matter scenarios, see [14], and see, for example, also [15–23] for further details regarding unified dark matter models.

The above scenarios are based on a Lagrangian and thus provide a physical justification of the models. However, because of the vast number of possible models, one can retreat to the pure phenomenological aspect. In this respect, one considers the dark energy as generalised dark matter in terms of the parameters  $c_{\text{eff}}$  and  $c_{\text{vis}}$  as defined in [1]. The UDM models require a dark matter component which has an equation of state  $w$  close to zero around the time of recombination. In addition, we will assume here that the equation of state will be almost zero deep in the radiation area. This contrasts to some tracker scenarios where the dark energy component behaves radiation-like in the radiation area. This paper focuses on early-matter-like dark energy which is defined by a dark energy component, whose equation of state vanishes at early times  $w_{\text{de}}(\eta = 0) = 0$  such that it can be expanded as

$$w_{\text{de}}(x) = w_1 x + w_2 x^2 + O(x^3) \quad \text{with} \quad x := \frac{a(\eta)}{A_0}, \quad (1.1)$$

where  $A_0$  denotes the current value of the scale factor  $a(\eta)$  so that  $x \in [0, 1]$ . It is the aim of this paper to provide power series of the perturbations of the various components in terms of the conformal time  $\eta$ . These allow the computation of the initial conditions for the numerical integration of the perturbations shortly before the recombination such that a tight-coupling approximation is not necessary. Although this Introduction emphasises UDM models, the power series is also computed for the usual cold dark matter component. Thus, the equations can also be applied to models dealing with dark matter and dark energy as two separated components provided that the equation of state of dark energy is given by (1.1). The algorithm is then applied to a phenomenological unified model which is suggested in [24] where the equation of state

$$w(z) = \frac{1}{\pi} \arctan(\alpha z - \beta) - \frac{1}{2} \quad (1.2)$$

is assumed with two parameters  $\alpha$  and  $\beta$ . It is shown in [24] that such a phenomenological dark fluid can describe the supernovae Ia data,  $\gamma$ -ray bursts and the baryon acoustic oscillations

for a parameter set around  $\alpha \simeq 2.14$  and  $\beta \simeq 0.95$ . Since this phenomenological dark fluid can describe these data, the question emerges whether this model predicts a power spectrum of the cosmic microwave background radiation according to cosmological observations.

## 2 The background model

In order to derive the power series of the perturbations, the power series of the scale factor  $a(\eta)$  of the background model has to be computed at first. Since the early-matter-like dark energy is important at early times, in contrast to models with a dark energy with  $w(\eta) < 0$ , the computation of the scale factor  $a(\eta)$  has to take the dark energy component into account. The energy density  $\varepsilon_{\text{de}}(\eta)$  evolves as

$$\begin{aligned} \varepsilon_{\text{de}}(\eta) &= \varepsilon_{\text{de}}^0 \exp \left( 3 \int_{x(\eta)}^1 \frac{1 + w_{\text{de}}(x)}{x} dx \right) \\ &= \varepsilon_{\text{de}}^0 \exp \left( 3 \int_0^1 \frac{w_{\text{de}}(x)}{x} dx \right) \exp \left( 3 \int_{x(\eta)}^1 \frac{dx}{x} \right) \\ &\quad \times \exp \left( -3 \int_0^{x(\eta)} \frac{w_{\text{de}}(x)}{x} dx \right) \\ &= \varepsilon_{\text{de}}^{\text{eff}} \left( \frac{A_0}{a(\eta)} \right)^3 \exp \left( -3 \int_0^{x(\eta)} \frac{w_{\text{de}}(x)}{x} dx \right) , \end{aligned} \tag{2.1}$$

where  $\varepsilon_{\text{de}}^0$  is the current energy density and we have defined

$$\varepsilon_{\text{de}}^{\text{eff}} := \varepsilon_{\text{de}}^0 \exp \left( 3 \int_0^1 \frac{w_{\text{de}}(x)}{x} dx \right) . \tag{2.2}$$

Note that in eqs. (2.1) and (2.2), the full expression of the equation of state has to be used and not only the early-times approximation (1.1). Furthermore, it is convenient to define

$$\Omega_{\text{de}}^{\text{eff}} := \frac{8\pi G}{3H_0^2 c^2} \varepsilon_{\text{de}}^{\text{eff}} \tag{2.3}$$

with the Hubble constant  $H_0$  and the gravitational constant  $G$ . The quantity  $\Omega_{\text{de}}^{\text{eff}}$  can be interpreted as the effective matter contribution of the UDM component at early times and should not be confused with the current value of the dark energy density  $\Omega_{\text{de}} = \frac{8\pi G}{3H_0^2 c^2} \varepsilon_{\text{de}}^0$ .

The Friedmann equation leads to the expansion of the scale factor  $a(\eta)$  in terms of the conformal time  $\eta$

$$a(\eta) = a_1 \eta + a_2 \eta^2 + a_3 \eta^3 + O(\eta^4) \tag{2.4}$$

with the coefficients

$$a_1 = \frac{H_0}{c} A_0^2 \sqrt{\Omega_{\text{rad}}} , \quad a_2 = \frac{1}{4} \left( \frac{H_0}{c} \right)^2 A_0^3 (\Omega_{\text{mat}} + \Omega_{\text{de}}^{\text{eff}}) \tag{2.5}$$

and

$$a_3 = \frac{1}{6} \left( \frac{H_0}{c} \right)^3 A_0^4 \sqrt{\Omega_{\text{rad}}} (\Omega_{\text{curv}} - 3w_1 \Omega_{\text{de}}^{\text{eff}}) \tag{2.6}$$

with the usual definitions of the present-day densities  $\Omega_{\text{rad}} = \Omega_\gamma + \Omega_\nu$ ,  $\Omega_{\text{mat}} = \Omega_{\text{bar}} + \Omega_{\text{cdm}}$  and  $\Omega_{\text{curv}}$ . In the case of UDM models, one has  $\Omega_{\text{cdm}} = 0$ . Equation (2.5) shows that  $\Omega_{\text{mat}}$  and  $\Omega_{\text{de}}^{\text{eff}}$  contribute in the same manner to the early-times behaviour of the scale factor. This expansion takes the early-matter-like dark energy into account and is used for the derivation of the power expansions of the perturbations of the various components.

### 3 Initial conditions and evolution of perturbations

The description of the perturbations requires the definition of the gauge. In this paper, we use the conformal Newtonian gauge, where the metric takes the form

$$ds^2 = a^2(\eta) \left\{ -(1 + 2\Psi)d\eta^2 + (1 + 2\Phi)\gamma_{ij}dx^i dx^j \right\} \quad (3.1)$$

and  $\gamma_{ij}$  denotes the spatial metric. The Newtonian metric perturbations are characterised by the two scalar potentials  $\Psi$  and  $\Phi$ . Note that the sign of  $\Phi$  differs from the definition used in [25] but is identical to the choice of [26].

In this paper, only isentropic initial conditions are considered which lead to initial perturbations in the relative energy density perturbations in dependence on the equation of state  $w_x$  at  $\eta = 0$  and on the initial perturbation of the potential  $\Psi_0$

$$\delta_{x,0} = -\frac{3}{2}(1 + w_x)\Psi_0 \quad . \quad (3.2)$$

These conditions are the natural outcome, if the primordial perturbations are generated from a single degree of freedom. This is the case in many inflationary scenarios where the decay of the inflaton leads to the stated isentropic initial conditions. In Appendix D, it is demonstrated that the initial conditions (3.2) lead to pure isentropic initial conditions without any isocurvature contribution.

The dynamical evolution of the perturbation of the dark component is not entirely fixed by specifying the initial condition (3.2) and the equation of state  $w_g$ , since this does not determine the pressure perturbation  $\delta p_g$  which is a priori unknown in this case. The equation of state  $p_g = w_g \varepsilon_g$  of the generalised dark matter component determines the adiabatic speed of sound as

$$c_g^2 = \frac{\dot{p}_g}{\dot{\varepsilon}_g} = w_g - \frac{1}{3} \frac{\dot{w}_g}{1 + w_g} \frac{a}{\dot{a}} \quad , \quad (3.3)$$

which enters the evolution equations. However, the entropy perturbation  $\Gamma$  is not fixed by specifying  $w_g$ . But this is necessary, since this quantity also occurs in the evolution equations of the density perturbation [1]

$$\dot{\delta}_g = -(1 + w_g)(kv_g + 3\dot{\Phi}) + \frac{\dot{w}_g}{1 + w_g} \delta_g - 3 \frac{\dot{a}}{a} w_g \Gamma \quad (3.4)$$

and of the velocity

$$\dot{v}_g = -\frac{\dot{a}}{a}(1 - 3c_g^2)v_g + \frac{c_g^2}{1 + w_g}k\delta_g + \frac{k w_g \Gamma}{1 + w_g} + k\Psi \quad , \quad (3.5)$$

where the scalar anisotropic stress amplitude is assumed to be zero. The entropy perturbation  $\Gamma$  occurring in eqs. (3.4) and (3.5) is related to the freedom of specifying the pressure perturbation [1, 27]. It is convenient to parameterise the entropy perturbation  $\Gamma$  by the effective

speed of sound  $c_{\text{eff}}^2$  as

$$\Gamma = \frac{c_{\text{eff}}^2 - c_g^2}{w_g} \delta_g^{(\text{rest})} , \quad (3.6)$$

where the density perturbation  $\delta_g^{(\text{rest})}$  in the rest frame of the generalised dark matter is determined by the transformation

$$\delta_g^{(\text{rest})} = \delta_g + 3 \frac{\dot{a}}{a} (1 + w_g) \frac{v_g}{k} . \quad (3.7)$$

If the effective speed of sound  $c_{\text{eff}}^2$  coincides with the adiabatic one  $c_g^2$ , the entropy perturbation  $\Gamma$  vanishes. The effective speed of sound  $c_{\text{eff}}^2$  is considered as a free parameter defining the evolution of the perturbations of the dark fluid. The effective speed of sound can be interpreted as the rest frame sound speed

$$c_{\text{eff}}^2 = \frac{\delta p_g^{(\text{rest})}}{\delta \rho_g^{(\text{rest})}} , \quad (3.8)$$

where  $\delta p_g^{(\text{rest})}$  and  $\delta \rho_g^{(\text{rest})}$  denote the pressure and density perturbations in the rest frame of the generalised dark matter component. This leads to a definition independent of the chosen gauge.

In order to compute the CMB anisotropy, one has to integrate a coupled system of differential equations. The numerical integration cannot start at  $\eta = 0$ , where the isentropic initial conditions (3.2) are posed, but only at a later time  $\eta_{\text{start}}$  before the recombination takes place at  $\eta_{\text{rec}}$  that is  $0 \ll \eta_{\text{start}} \ll \eta_{\text{rec}}$ . To ensure that the isentropic initial conditions (3.2) defined at  $\eta = 0$  are correctly taken into account at  $\eta_{\text{start}}$ , a power series expansion for each of the perturbations is used. Since the system of differential equations is coupled, there is no direct way of obtaining such power series. Instead one has to carry out a step by step calculation to eliminate the unwanted quantities. The strategy of finding the appropriate solutions is to express the expansion coefficients of the potentials  $\Psi(\eta)$  and  $\Phi(\eta)$  solely in terms of the background model that is in terms of the coefficients given in (2.5) and (2.6). These potential expansions are given in Appendix A. Then, the second step is to express the power series of the perturbations of the various energy components solely in terms of the expansion coefficients of the potentials  $\Psi(\eta)$  and  $\Phi(\eta)$ . In this way, the start values at  $\eta_{\text{start}}$  are obtained by computing at first the coefficients of the potentials  $\Psi(\eta)$  and  $\Phi(\eta)$  given in Appendix A and thereafter, from the known potentials, the perturbations  $\delta_x(\eta_{\text{start}})$  and  $v_x(\eta_{\text{start}})$ . Their power series are given in Appendix B and Appendix C in terms of the potentials. After all start values are computed at  $\eta_{\text{start}}$  from the primordial initial values at  $\eta = 0$ , the numerical integration is carried out with the evolution equations which are also given in Appendices A, B and C. The metric and energy density perturbations allow the computation of the CMB anisotropy along the lines given in [25, 26]. In contrast to public domain programs for the computation of the CMB power spectrum, our code uses the conformal Newtonian gauge instead of the synchronous gauge.

It should be noted that in [28] the series expansion of the potentials is derived by transforming the corresponding result obtained in the synchronous gauge into the conformal Newtonian gauge. However, their result differs from that in Appendix A since the gauge transformation requires the synchronous gauge result two order higher than used in [28].

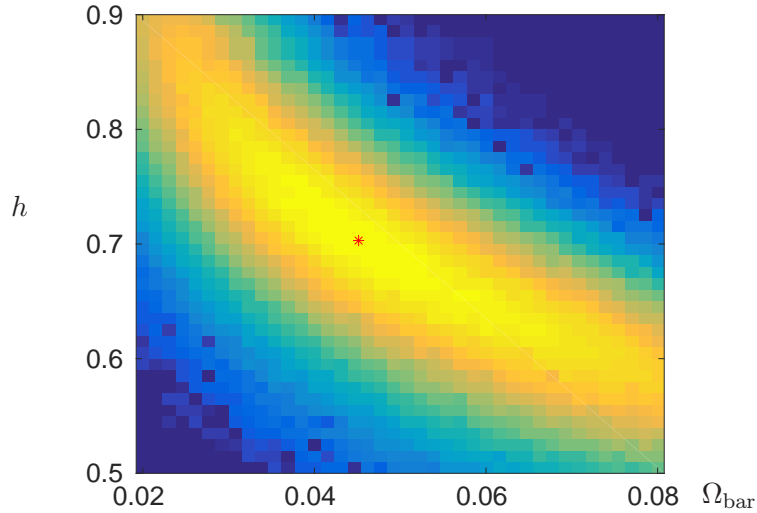


**Figure 1.** The likelihood is plotted in the  $\Omega_{\text{bar}} - h$  plane. The best-fit model is marked by the star.

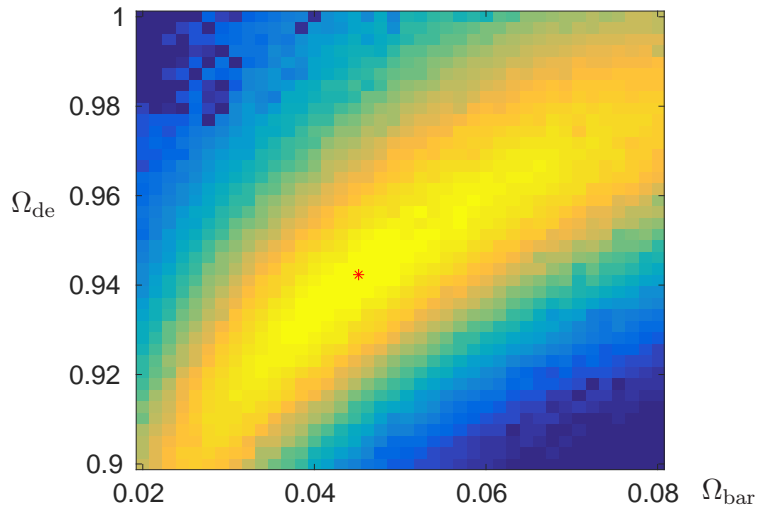


**Figure 2.** The likelihood is plotted in the  $\Omega_{\text{bar}} - \Omega_{\text{de}}$  plane. The best-fit model is marked by the star.

#### 4 CMB anisotropy for the arctan-UDM model

In this section, we apply our program to the phenomenological UDM model proposed in [24] in order to compute the CMB power spectrum. The equation of state of this UDM component is already defined in eq.(1.2). The parameters in the equation of state (1.2) are fixed at  $\alpha = 2.14$  and  $\beta = 0.95$ , since these values are in accordance with the supernovae Ia data,  $\gamma$ -ray bursts and the baryon acoustic oscillations as demonstrated in [24]. The equation of state (1.2) leads for the expansion (1.1) to the coefficients

$$w_1 = -\frac{1}{\pi \alpha} \quad \text{and} \quad w_2 = -\frac{\alpha + \beta}{\pi \alpha^2}, \quad (4.1)$$

which have to be used for the computation of the start values at  $\eta_{\text{start}}$  as discussed above.

With the given values of  $\alpha$  and  $\beta$ , a Markov chain Monte Carlo (MCMC) sequence of models is generated where  $\Omega_{\text{bar}}$ ,  $\Omega_{\text{de}}$  and the reduced Hubble constant  $h$  are varied. The

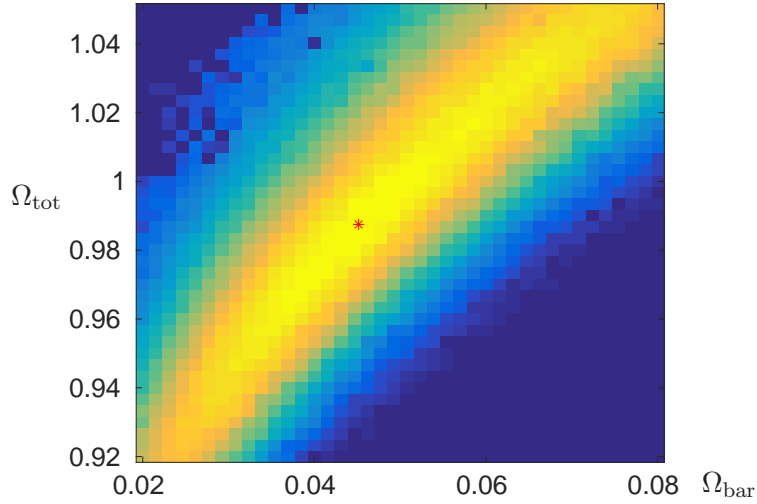


**Figure 3.** The likelihood is plotted in the  $\Omega_{\text{bar}} - \Omega_{\text{tot}}$  plane. The best-fit model is marked by the star.

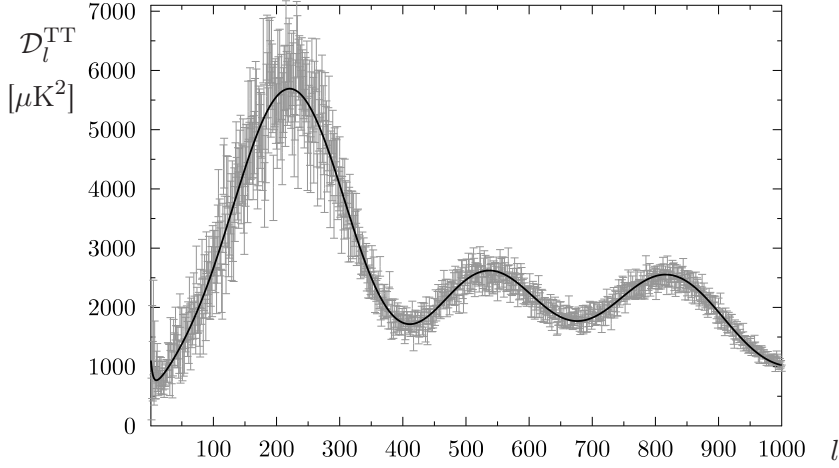


**Figure 4.** The angular power spectrum  $\mathcal{D}_l^{\text{TT}} = l(l+1)C_l^{\text{TT}}/(2\pi)$  is plotted using the values of the best-fit model as stated in the text. The  $\mathcal{D}_l^{\text{TT}}$  measurements of the Planck 2015 data release [29] are plotted with the corresponding error bars.

other cosmological parameters are held fixed at values taken from the  $\Lambda$ CDM concordance model. The  $\Lambda$ CDM model with the parameters given in Table 9 in [29] designated as “Planck TT+lowP+lensing” is used in this paper. The cosmological parameters of the  $\Lambda$ CDM model are  $\Omega_{\text{bar}} = 0.0484$ ,  $\Omega_{\text{cdm}} = 0.258$ ,  $\Omega_{\Lambda} = 0.6935$ , the reduced Hubble constant  $h = 0.678$ , the reionisation optical depth  $\tau = 0.066$ , and the scalar spectral index  $n_s = 0.9677$ . In our UDM model, the densities  $\Omega_{\text{cdm}}$  and  $\Omega_{\Lambda}$  are set to zero since they are unified in the component denoted by  $\Omega_{\text{de}}$ . For the reionisation optical depth, the value  $\tau = 0.066$  is used. Furthermore, the scalar spectral index  $n_s$  and the overall normalisation factor are fitted so that a best-fit is obtained to the angular power spectrum  $\mathcal{D}_l^{\text{TT}} := l(l+1)C_l^{\text{TT}}/(2\pi)$  of the Planck 2015 data release [29]. The UDM model power spectra  $\mathcal{D}_l^{\text{TT}}$  are fitted over the interval  $2 \leq l \leq 1000$  to the Planck data.



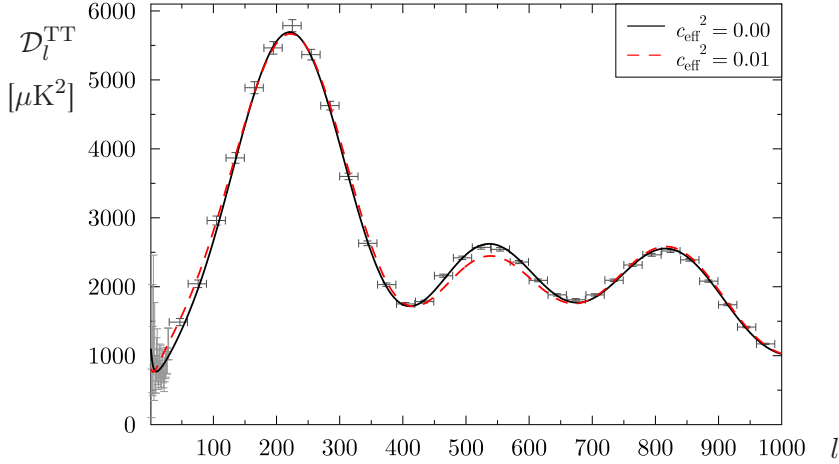


**Figure 5.** The angular power spectrum  $\mathcal{D}_l^{\text{TT}}$  is shown for the best-fit model as stated in the text. The binned data of the Planck 2015 data release [29] are plotted for  $l > 30$  with the corresponding error bars. In addition, the angular power spectrum is shown for a model where in contrast to the best-fit model the effective speed of sound is slightly enhanced to  $c_{\text{eff}}^2 = 0.01$ . This leads to a reduced second acoustic peak due to a different normalisation and spectral index.

Furthermore, for this MCMC sequence, the value of the effective speed of sound  $c_{\text{eff}}^2$  is set to zero. It is discussed below that non-zero values lead to the same problems as in other UDM models as, for example, the generalised Chaplygin gas. The likelihood distribution is shown in figures 1 to 3 where the reduced Hubble constant  $h$ , the density of the dark energy  $\Omega_{\text{de}}$ , and the total energy density  $\Omega_{\text{tot}}$  are shown in dependence on  $\Omega_{\text{bar}}$ , respectively. The best-fit model of this MCMC sequence has the cosmological parameters  $h = 0.703$ ,  $\Omega_{\text{bar}} = 0.0451$ ,  $\Omega_{\text{de}} = 0.942$ ,  $n_s = 0.975$ . These parameters lead to an effective early dark matter contribution of  $\Omega_{\text{de}}^{\text{eff}} = 0.2267$  which is defined in (2.3). The best-fit model is marked by a star in figures 1 to 3. The corresponding angular power spectrum  $\mathcal{D}_l^{\text{TT}}$  is shown in figure 4 in comparison to the unbinned Planck data [29]. The good agreement with the data is clearly visible. A comparison with the binned Planck data is presented in figure 5 which again reveals the agreement. This plot also demonstrates the influence of a dark matter component with a non-vanishing effective speed of sound, where the very small value  $c_{\text{eff}}^2 = 0.01$  is used.

The optical depth  $\tau$  to the surface of last scattering has changed from  $\tau = 0.089 \pm 0.032$  of the Planck 2013 analysis [30] to  $\tau = 0.066 \pm 0.016$  of the 2015 analysis [29]. In order to test the influence of this change, we also generate a MCMC sequence of models, where the optical depth  $\tau$  is fixed by the higher value of  $\tau = 0.091$ . It turns out, that this change does not alter the results, since the best model possesses almost the same cosmological parameters as those of the  $\tau = 0.066$  run. Both model curves are shown in figure 6, where a logarithmic scaling in  $l$  is chosen since the main difference occurs at low values of  $l$ . It is seen that the curves are almost indistinguishable.

The analysis of [24] for the UDM model does not require assumptions on the effective speed of sound  $c_{\text{eff}}^2$ . Their analysis tests the agreement with the supernovae Ia data, the baryon acoustic oscillations and the gamma-ray data, and these tests are based on the background model providing the luminosity distance and the angular diameter distance. So it suffice to specify the equation of state (1.2) for the UDM component. The comparison with the CMB

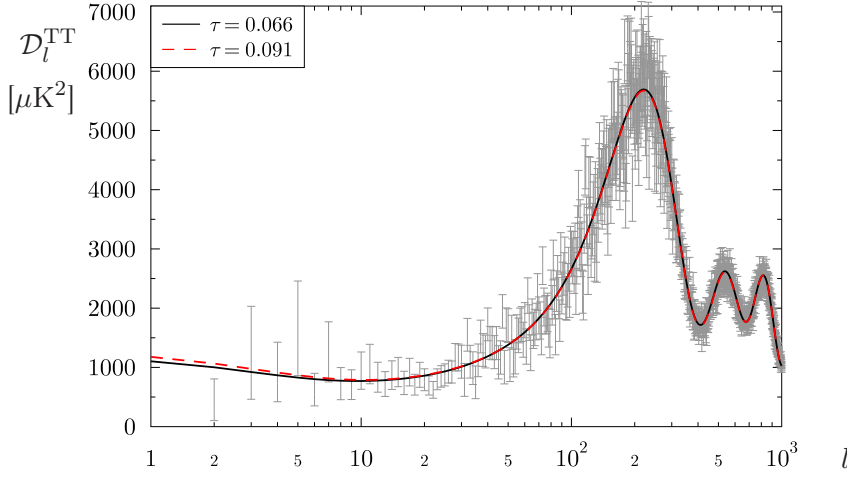


**Figure 6.** The angular power spectrum  $\mathcal{D}_l^{\text{TT}}$  is plotted for the same model as in figure 4 but now with a logarithmic scaling on the  $l$  axis so that the agreement at low values of  $l$  can be seen. In addition, the best-fit model for the higher optical depth  $\tau = 0.091$  is shown as a dashed curve.

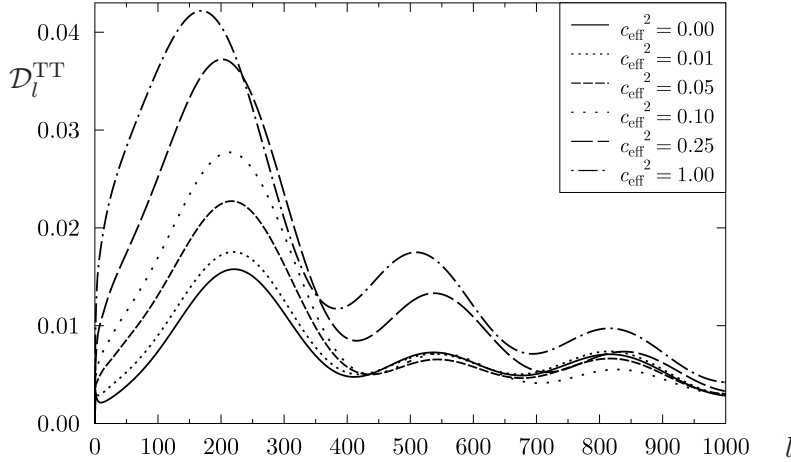


**Figure 7.** The angular power spectrum  $\mathcal{D}_l^{\text{TT}}$  is shown in dependence on the effective speed of sound  $c_{\text{eff}}^2$ . All other cosmological parameters are kept constant with the values of the best-fit model. The same initial power power spectrum is used for all curves and no fit to the cosmological data is performed.

data requires the additional specification of the effective speed of sound  $c_{\text{eff}}^2$ . As discussed in the Introduction, other UDM models, especially the generalised Chaplygin gas model, have difficulties to match the behaviour of cosmological perturbations in the case of a non-vanishing effective speed of sound. In our main MCMC computation, we set  $c_{\text{eff}}^2 = 0$  as discussed above. However, also a shorter MCMC sequence is generated without this restriction and reveals the preference for almost zero values of  $c_{\text{eff}}^2$ . Figure 5 shows a comparison of two models which differ only in the effective speed of sound  $c_{\text{eff}}^2$ . The values  $c_{\text{eff}}^2 = 0$  and  $c_{\text{eff}}^2 = 0.01$  are shown, and one observes a decline of the second acoustic peak and an increasing amplitude towards small values of  $l$  for the curve with  $c_{\text{eff}}^2 = 0.01$ . However, these changes are mainly caused

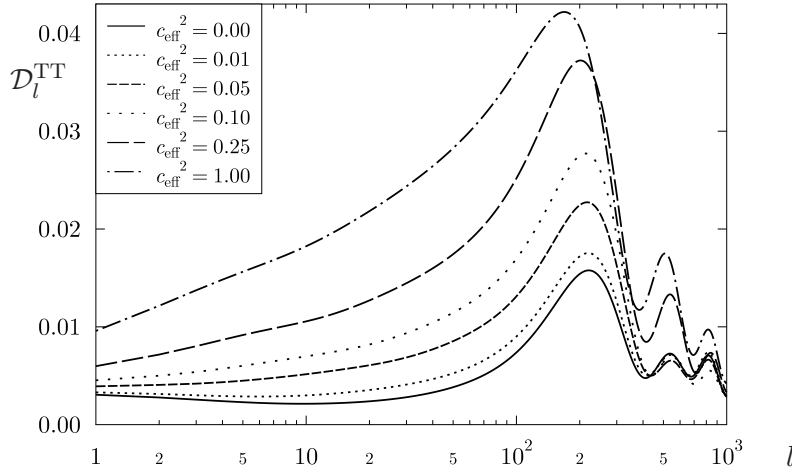


**Figure 8.** The same curves as in figure 7 are shown but now with a logarithmic scaling on the  $l$  axis in order to emphasise the late ISW contribution.

by fitting the model curve to the CMB data. Because of the increase of the amplitude at and prior to the first acoustic peak, one obtains a smaller overall normalisation factor and a higher spectral index  $n_s$ , which leads to a suppressed amplitude of the second peak and an almost invariant amplitude of the third peak for the two values of  $c_{\text{eff}}^2$ .

In order to avoid the influence of the normalisation factor and the spectral index  $n_s$ , we show in figures 7 and 8 the angular power spectrum  $\mathcal{D}_l^{\text{TT}}$  which is not fitted to the data. These power spectra are computed from the same primordial power spectrum, so that the genuine effect of the effective speed of sound  $c_{\text{eff}}^2$  can be seen. All other cosmological parameters are those of the stated best-fit model. These plots reveal the large increase at small values of  $l$  due to the integrated Sachs-Wolfe effect [11, 14]. This is clearly visible in figure 8, where a logarithmic scaling is chosen for  $l$ . Also the first acoustic peak increases significantly, the amplitude of the second and third peak are relatively insensitive for not too large values of  $c_{\text{eff}}^2$ . For  $c_{\text{eff}}^2 = 1$ , which would be the quintessence value, the angular power spectrum looks very distorted compared to the structure required by the data. It is noteworthy that all curves are computed for the same background model, so that the same relations between the redshift and luminosity distance or the angular diameter distance are obtained.

Our MCMC algorithm computes the probability needed for the model sequence only from the temperature angular power spectrum  $\mathcal{D}_l^{\text{TT}}$ , so the match with the polarization data is completely ignored for the generation of the MCMC sequence. However, it is nevertheless important to compare the Planck polarization data [29] with the spectrum of the best-fit model. In figure 9, the polarization power spectra  $\mathcal{D}_l^{\text{TE}} := l(l+1)C_l^{\text{TE}}/(2\pi)$  and  $\mathcal{D}_l^{\text{EE}} := l(l+1)C_l^{\text{EE}}/(2\pi)$  are shown in panels (a) and (b), respectively, in comparison to the binned TE and EE data of the Planck 2015 data release [29]. The best-fit model with  $c_{\text{eff}}^2 = 0$  is plotted as a full curve, while the model with the slightly enhanced value of  $c_{\text{eff}}^2 = 0.01$  is shown as the dashed curve. With respect to the fact that the best-fit model is solely determined from the temperature power spectrum  $\mathcal{D}_l^{\text{TT}}$ , it is assuring that also the polarization data agree well with the best-fit model. The comparison with the model with  $c_{\text{eff}}^2 = 0.01$  reveals discrepancies as it is the case for the temperature power spectrum  $\mathcal{D}_l^{\text{TT}}$  shown in figure 5. The largest deviations can be found for the EE spectrum around  $l \simeq 700$ .

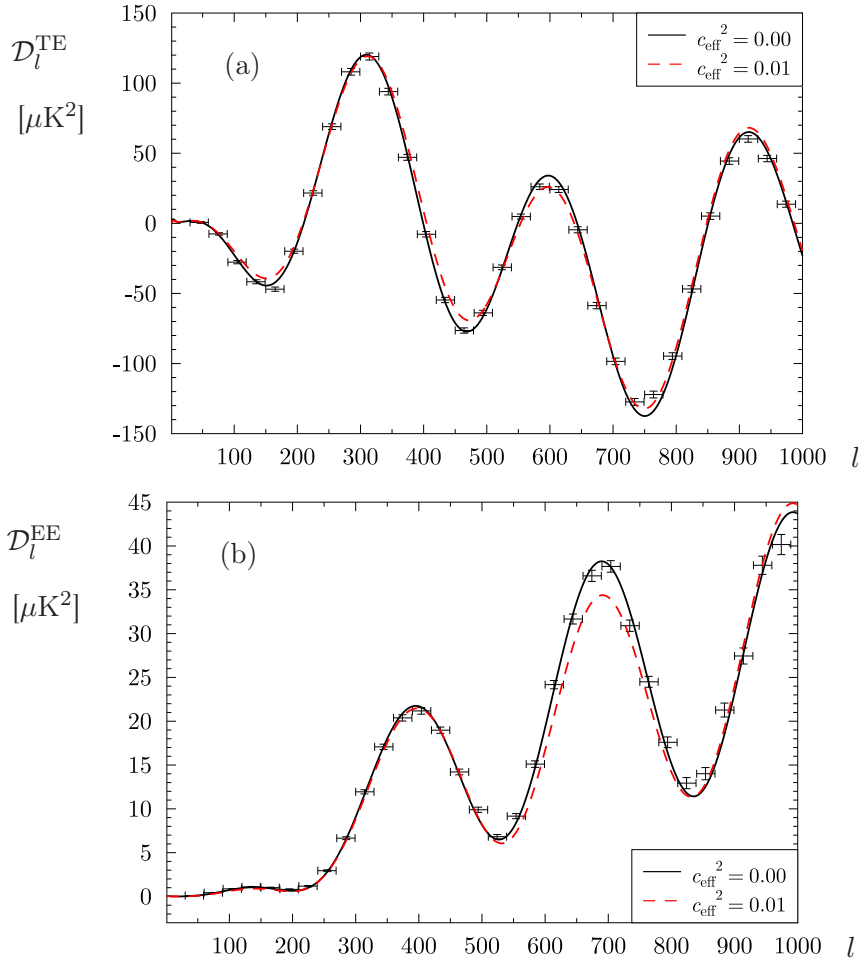


**Figure 9.** The polarization power spectra  $\mathcal{D}_l^{\text{TE}} = l(l+1)C_l^{\text{TE}}/(2\pi)$  and  $\mathcal{D}_l^{\text{EE}} = l(l+1)C_l^{\text{EE}}/(2\pi)$  are shown in panels (a) and (b), respectively, for the best-fit model as stated in the text. The binned TE and EE data of the Planck 2015 data release [29] are plotted with the corresponding error bars. In addition, the polarization power spectra are shown for the model with the slightly increased effective speed of sound  $c_{\text{eff}}^2 = 0.01$ .

As discussed in the case of the temperature power spectrum, the fit to the Planck data hides the genuine effect of the effective speed of sound  $c_{\text{eff}}^2$  on the polarization power spectra. Thus, in contrast to figure 9, the figure 10 shows the polarization power spectra  $\mathcal{D}_l^{\text{TE}}$  and  $\mathcal{D}_l^{\text{EE}}$  for the same set of cosmological parameters with the exception of  $c_{\text{eff}}^2$  which is varied from zero to one. As discussed above, the temperature power spectrum shown in figures 7 and 8 is most sensitive at and below the first acoustic peak to small changes in  $c_{\text{eff}}^2$  for  $c_{\text{eff}}^2 \lesssim 0.1$ . This behaviour differs from the polarization spectra. The inspection of figure 10 reveals the general trend that the polarization amplitude increases with increasing  $c_{\text{eff}}^2$ . This increase in polarization power is also noticeable around the second peak of the EE spectrum. However, the systematic increase is not observed around the third peak. The cross-power spectrum  $\mathcal{D}_l^{\text{TE}}$  displays a signature of the value of  $c_{\text{eff}}^2$  for  $l \lesssim 20$  as shown by the inset of figure 10(a) which appears in the main figure as a small spike.

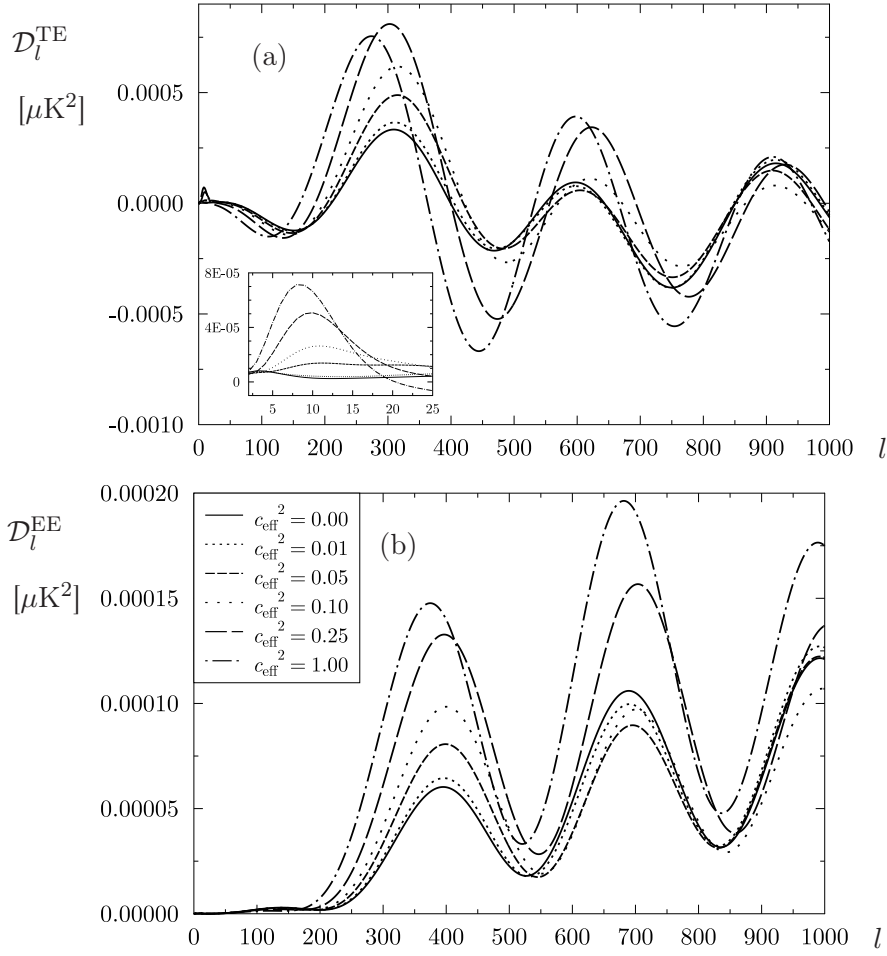


**Figure 10.** The polarization power spectra  $\mathcal{D}_l^{\text{TE}}$  and  $\mathcal{D}_l^{\text{EE}}$  are shown in panels (a) and (b), respectively, in dependence on the effective speed of sound  $c_{\text{eff}}^2$ . With the exception of  $c_{\text{eff}}^2$ , all other cosmological parameters are held fixed as those of the best-fit model. Since no fit to the Planck data is carried out, these two panels reveal the effect of  $c_{\text{eff}}^2$  on the polarization power spectra. The legend of panel (b) applies also to panel (a).

## 5 Summary

In this paper, the CMB anisotropy is computed for a phenomenological unified dark matter (UDM) model, where the behaviour of the cold dark matter and of the cosmological constant of the  $\Lambda$ CDM model is represented by a single component. At early times the UDM behaviour mimics that of cold dark matter, and thus, this component might be called early-matter-like dark energy. It changes the cosmological background model by modifying the scale factor already at early times. This in turn influences the growth of the perturbations of the metric and the various energy components. In order to compute the CMB anisotropy, an expansion of the scale factor in terms of the conformal time is derived. It is used for a power series expansion in terms of the conformal time of the metric perturbations as well as of the energy perturbations for all components. These series expansions are given in the Appendix. This allows to start the numerical integration of the Boltzmann hierarchy for the

computation of the CMB anisotropy at sufficiently late times, since the start values for the numerical integration are computed from the corresponding power series. In this way the isentropic initial conditions are accurately taken into account. Simultaneously, this procedure circumvents numerical accuracy problems at very small conformal times.

The algorithm is applied to the phenomenological arctan-UDM scenario which is analysed in [24]. This model is defined by the equation of state (1.2) which is parameterised by two coefficients  $\alpha$  and  $\beta$ . The UDM model is compared in [24] with supernovae Ia data, the baryon acoustic oscillations and gamma-ray data, and it is found that a good agreement is achieved for  $\alpha \simeq 2.14$  and  $\beta \simeq 0.95$ . Since their analysis does not discuss the CMB anisotropy, we apply our CMB algorithm to their UDM model in this work. It is indeed found that there is a parameter range for which the CMB anisotropy agrees with the Planck 2015 data [29], if one allows for a vanishing effective speed of sound  $c_{\text{eff}}^2$  which is defined in (3.6). This is consistent with the lesson from the generalised Chaplygin gas model, which predicts a wrong evolution of the perturbations except one allows the generation of entropy perturbations.

In [31] a great plethora of dark energy models is analysed with respect to the Planck 2015 data. One important implication is that the density of dark energy at early times has to be below 2% of the critical density using only the Planck data. Taking other data into account, [31] reports the even lower bound  $\Omega_{\text{de}}(\eta) < 0.0071$  (95% CL, Planck TT+lensing+BAO+SNe+ $H_0$ ) at early times. Although the arctan-UDM model has a significantly larger value of  $\Omega_{\text{de}}(\eta)$  at early times, it elegantly escapes this bound, because its equation of state (1.2) has already changed to that of a CDM component at the relevant times. This loophole is emphasised by the figures 4 and 5, which reveal the good match between the theoretical prediction and the Planck 2015 observations of the temperature CMB angular power spectrum. For the same set of cosmological parameters, the arctan-UDM model also predicts polarization spectra that agree with the Planck data as shown in figure 9. This agreement is, however, spoiled if the effective speed of sound  $c_{\text{eff}}^2$  is not very close to zero. So the conclusion is that UDM models can match the observed CMB anisotropy if the effective speed of sound is almost zero.

## Appendix

### A The power series of the potentials in conformal time

The evolution equations of the Newtonian metric perturbations  $\Psi$  and  $\Phi$  are given in Fourier space by (see, e.g. [26])

$$3 \left( \frac{a'(\eta)}{a(\eta)} \right)^2 \Psi(\eta) - 3 \frac{a'(\eta)}{a(\eta)} \Phi'(\eta) - K_2 k^2 \Phi = - \frac{4\pi G}{c^2} a^2(\eta) \rho_T(\eta) \delta_T(\eta) \quad , \quad (\text{A.1})$$

$$\frac{a'(\eta)}{a(\eta)} \Psi(\eta) - \Phi'(\eta) = \frac{4\pi G}{c^2} a^2(\eta) \left( \rho_T(\eta) + p_T(\eta)/c^2 \right) \frac{v_T(\eta)}{k} \quad , \quad (\text{A.2})$$

and

$$k^2(\Psi(\eta) + \Phi(\eta)) = - \frac{8\pi G}{c^4} a^2(\eta) p_T(\eta) \Pi_T(\eta) \quad . \quad (\text{A.3})$$

Here,  $\rho_T(\eta)$ ,  $p_T(\eta)$ ,  $v_T(\eta)$ , and  $\Pi_T(\eta)$  are the matter density, the pressure, the velocity, and the anisotropic stress perturbation in the total matter gauge, respectively, as defined in [26]. Furthermore, the quantity  $K_2$  in eq. (A.1) is defined by

$$K_l := 1 - (l^2 - 1)K/k^2 \quad \text{with the curvature constant} \quad K \in \{-1, 0, +1\} \quad ,$$

for a hyperbolic, flat, or spherical space, respectively. The wave number  $k$  is related to the eigenvalue  $E$  of the Laplace-Beltrami operator by  $k = \sqrt{E} = \sqrt{\beta^2 - K}$ . In the case of positive curvature, the eigenvalue spectrum is discrete  $\beta = 3, 4, 5, \dots$ . For a flat space  $K = 0$  or for a negatively curved space  $K = -1$ , one has  $\beta \in \mathbb{R}^+$ .

The potentials are expanded up to second order

$$\Phi(\eta) = \Phi_0 + \Phi_1\eta + \frac{1}{2}\Phi_2\eta^2 + O(\eta^3) \quad (\text{A.4})$$

and

$$\Psi(\eta) = \Psi_0 + \Psi_1\eta + \frac{1}{2}\Psi_2\eta^2 + O(\eta^3) \quad (\text{A.5})$$

Imposing the isentropic initial conditions (3.2), these expansion coefficients are obtained as

$$\Psi_0 = -\frac{\Phi_0}{1 + \frac{2}{5}f_\nu} \quad \text{with the neutrino energy fraction} \quad f_\nu := \frac{\Omega_\nu}{\Omega_{\text{rad}}} \quad (\text{A.6})$$

and  $\Phi_0$  is determined by the initial power spectrum. The next order is derived as

$$\Phi_1 = \frac{\frac{a_2}{a_1} \left(1 + \frac{16}{15}f_\nu\right) - \frac{16}{15}\frac{a_1^2}{d}(1 - f_\nu)}{4 + \frac{8}{15}f_\nu} \Psi_0 \quad (\text{A.7})$$

and

$$\Psi_1 = 3\Phi_1 - \frac{a_2}{a_1} \Psi_0 \quad (\text{A.8})$$

The potentials depend on the perturbations in the various energy components, and thus, the derivation of (A.7) and (A.8) already requires the solutions of the corresponding energy perturbation equations in terms of the conformal time  $\eta$ . In these equations occur the optical depth for which the approximation  $\dot{\tau} = d/a^2(\eta)$  is used where  $d$  is a constant for  $\eta \ll \eta_{\text{rec}}$ .

The second-order terms are more involved and we define the quantities

$$Q_2 := \frac{1}{3}k^2 K_2(2\Phi_0 - \Psi_0) + 6\frac{a_2}{a_1}(2\Phi_1 - \Psi_1) + \left(\frac{2}{3}k^2 - 6\frac{a_3}{a_1}\right) \Psi_0$$

and

$$\begin{aligned} R_2 := & -2 \left( \left( \frac{a_2}{a_1} \right)^2 + 2\frac{a_3}{a_1} \right) (\Phi_0 + \Psi_0) - 4\frac{a_2}{a_1}(\Phi_1 + \Psi_1) \\ & - \frac{16}{15}(1 - f_\nu)\frac{a_1}{d^2} \{ (2da_2 - 11a_1^3)\Psi_0 + 4da_1\Phi_1 \} \\ & + \frac{k^2}{45}f_\nu \left( 1 + \frac{4}{5}K_2 + \frac{27}{35}K_3 \right) \Psi_0 \end{aligned}$$

in order to write

$$\Phi_2 = \frac{R_2 - (1 + \frac{2}{15}f_\nu)Q_2}{5 + \frac{2}{5}f_\nu} \quad \text{and} \quad \Psi_2 = 4\Phi_2 + Q_2 \quad (\text{A.9})$$

If the initial condition  $\Phi_0$  is chosen, the expansions (A.4) and (A.5) can thus be computed solely from background model data that is from the coefficients  $a_1$ ,  $a_2$  and  $a_3$ .

## B The generalised matter perturbations in terms of the potentials

The differential equations for the generalised dark matter perturbations, given in eqs. (3.4) and (3.5), can be rewritten for the density perturbation as (see [1])

$$\dot{\delta}_g = -(1 + w_g)(kv_g + 3\dot{\Phi}) - 3\frac{\dot{a}}{a}(c_{\text{eff}}^2 - w_g)\delta_g^{(\text{rest})} - 3\frac{\dot{a}}{a}\dot{w}_g\frac{v_g}{k} \quad (\text{B.1})$$

and for the velocity as

$$\dot{v}_g = -\frac{\dot{a}}{a}v_g + \frac{c_{\text{eff}}^2}{1 + w_g}k\delta_g^{(\text{rest})} + k\Psi, \quad (\text{B.2})$$

where the density perturbation in the rest frame of the generalised dark matter is defined in (3.7). The generalised dark matter perturbation is expanded as

$$\delta_g(\eta) = \delta_{g,0} + \delta_{g,1}\eta + \frac{1}{2}\delta_{g,2}\eta^2 + O(\eta^3) \quad (\text{B.3})$$

and the coefficients are calculated as

$$\delta_{g,0} = -\frac{3}{2}\Psi_0, \quad \delta_{g,1} = -3\Phi_1 - \frac{3}{2}\frac{a_1}{A_0}w_1\Psi_0 \quad (\text{B.4})$$

and

$$\begin{aligned} \delta_{g,2} = & -3\left[\Phi_2 + \frac{k^2}{6}\Psi_0 + \frac{c_{\text{eff}}^2}{4 + 3c_{\text{eff}}^2}\frac{k^2}{2}K_2(2\Phi_0 - \Psi_0)\right] \\ & - 3w_1\left(\frac{a_2}{A_0}\Psi_0 + 2\frac{a_1}{A_0}\Phi_1\right) - 3w_2\frac{a_1^2}{A_0^2}\Psi_0. \end{aligned} \quad (\text{B.5})$$

These coefficients are derived for an equation of state as given in (1.1) where also the coefficients  $w_1$  and  $w_2$  are defined.

Expanding the velocity perturbations analogously as

$$v_g(\eta) = v_{g,1}\eta + \frac{1}{2}v_{g,2}\eta^2 + \frac{1}{6}v_{g,3}\eta^3 + O(\eta^4) \quad (\text{B.6})$$

leads with (B.2) to

$$v_{g,1} = \frac{k}{2}\Psi_0, \quad v_{g,2} = k(\Psi_1 - \Phi_1) \quad (\text{B.7})$$

and

$$v_{g,3} = k\left[\Psi_2 - \Phi_2 - \frac{k^2}{6}\left[\Psi_0 + \frac{2 - 3c_{\text{eff}}^2}{4 + 3c_{\text{eff}}^2}K_2(2\Phi_0 - \Psi_0)\right]\right]. \quad (\text{B.8})$$

These expansions are valid for all non-interacting fluids and those of the cold dark matter are obtained from the generalised dark matter equations by setting  $c_{\text{eff}}^2 = w_1 = w_2 = 0$ . This leads to

$$\delta_{\text{cdm},0} = -\frac{3}{2}\Psi_0, \quad \delta_{\text{cdm},1} = -3\Phi_1 \quad \text{and} \quad \delta_{\text{cdm},2} = -3\Phi_2 - \frac{k^2}{2}\Psi_0 \quad (\text{B.9})$$

and

$$\begin{aligned} v_{\text{cdm},1} &= \frac{k}{2}\Psi_0, \quad v_{\text{cdm},2} = k(\Psi_1 - \Phi_1) \\ \text{and} \quad v_{\text{cdm},3} &= k\left[\Psi_2 - \Phi_2 - \frac{k^2}{6}\left[\Psi_0 + \frac{K_2}{2}(2\Phi_0 - \Psi_0)\right]\right]. \end{aligned} \quad (\text{B.10})$$



The velocity equation of the baryonic matter differs from (B.2) by the additional interaction term  $\dot{\tau}(\Theta_1 - v_{\text{bar}})/R$  with  $R = 3\varepsilon_{\text{bar}}/4\varepsilon_\gamma$  due to the Compton scattering. Up to the considered order, the density perturbations are the same as in the case of cold dark matter, eqs. (B.9),

$$\delta_{\text{bar},0} = -\frac{3}{2}\Psi_0, \quad \delta_{\text{bar},1} = -3\Phi_1 \quad \text{and} \quad \delta_{\text{bar},2} = -3\Phi_2 - \frac{k^2}{2}\Psi_0, \quad (\text{B.11})$$

but the third order term in the velocity perturbation differs

$$v_{\text{bar},1} = \frac{k}{2}\Psi_0, \quad v_{\text{bar},2} = k(\Psi_1 - \Phi_1) \quad \text{and} \quad v_{\text{bar},3} = \Theta_{1,3} \quad (\text{B.12})$$

with  $\Theta_{1,3}$  given in (C.11).

## C The radiation perturbations in terms of the potentials

From the Boltzmann hierarchy of the photon perturbations  $\Theta_l$ , we need for our small  $\eta$  expansion only the first four equations (see [26])

$$\dot{\Theta}_0 = -\frac{k}{3}\Theta_1 - \dot{\Phi}, \quad (\text{C.1})$$

$$\dot{\Theta}_1 = k\left[\Theta_0 + \Psi - \frac{2}{5}\sqrt{K_2}\Theta_2\right] - \dot{\tau}(\Theta_1 - v_{\text{bar}}), \quad (\text{C.2})$$

$$\dot{\Theta}_2 = k\left[\frac{2}{3}\sqrt{K_2}\Theta_1 - \frac{3}{7}\sqrt{K_3}\Theta_3\right] - \dot{\tau}\left(\frac{9}{10}\Theta_2 - \frac{\sqrt{6}}{10}E_2\right), \quad (\text{C.3})$$

$$\dot{\Theta}_3 = k\left[\frac{3}{5}\sqrt{K_3}\Theta_2 - \frac{4}{9}\sqrt{K_4}\Theta_4\right] - \dot{\tau}\Theta_3. \quad (\text{C.4})$$

The density perturbation of the photons is defined as  $\Theta_0 := \frac{1}{4}\delta_\gamma$ . For the polarization, the equations of the first two  $E$  modes are required

$$\dot{E}_2 = -k\frac{\sqrt{5}}{7}\sqrt{K_3}E_3 - \dot{\tau}\left(\frac{4}{10}E_2 - \frac{\sqrt{6}}{10}\Theta_2\right) \quad (\text{C.5})$$

and

$$\dot{E}_3 = k\left[\frac{1}{\sqrt{5}}\sqrt{K_3}E_2 - \frac{\sqrt{12}}{9}\sqrt{K_4}E_4\right] - \dot{\tau}E_3. \quad (\text{C.6})$$

The perturbations  $\Theta_l$  for  $l = 0, 1, 2, 3$  are expanded as

$$\Theta_l(\eta) = \sum_{j=l}^{l+2} \frac{\Theta_{l,j}}{j!} \eta^j + O(\eta^{l+3}) \quad (\text{C.7})$$

and of  $E_l$  for  $l = 2, 3$  as

$$E_l(\eta) = \sum_{j=l}^{l+2} \frac{E_{l,j}}{j!} \eta^j + O(\eta^{l+3}). \quad (\text{C.8})$$

The evaluation of the differential equations leads for isentropic initial conditions for  $l = 0$  to

$$\Theta_{0,0} = -\frac{1}{2}\Psi_0, \quad \Theta_{0,1} = -\Phi_1 \quad \text{and} \quad \Theta_{0,2} = -\Phi_2 - \frac{k^2}{6}\Psi_0 \quad (\text{C.9})$$

for  $l = 1$  to

$$\Theta_{1,1} = \frac{k}{2} \Psi_0 \quad , \quad \Theta_{1,2} = k(\Psi_1 - \Phi_1) \quad (C.10)$$

$$\text{and} \quad \Theta_{1,3} = k \left[ \Psi_2 - \Phi_2 - \frac{k^2}{6} \Psi_0 \right] \quad (C.11)$$

and for  $l = 2$  to

$$\Theta_{2,2} = 0 \quad , \quad \Theta_{2,3} = \frac{8}{3} k^2 \sqrt{K_2} \frac{a_1^2}{d} \Psi_0 \quad \text{and} \quad (C.12)$$

$$\Theta_{2,4} = \frac{16k^2 \sqrt{K_2} a_1}{3d^2} \{ (2da_2 - 11a_1^3) \Psi_0 + 4da_1 \Phi_1 \} \quad .$$

For the  $E$  mode, one finds for the relevant non-vanishing coefficients

$$E_{2,3} = \sqrt{\frac{8}{3}} \frac{k^2 \sqrt{K_2} a_1^2}{d} \Psi_0 \quad \text{and} \quad E_{2,4} = \frac{8\sqrt{\frac{2}{3}} k^2 \sqrt{K_2} a_1}{d^2} \{ (da_2 - 13a_1^3) \Psi_0 + 2da_1 \Phi_1 \} \quad .$$

The expansions for the neutrino perturbations are defined analogously to the photons

$$N_l(\eta) = \sum_{j=l}^{l+2} \frac{N_{l,j}}{j!} \eta^j + O(\eta^{l+3}) \quad . \quad (C.13)$$

The differential equations for the neutrinos are obtained from (C.1) to (C.4) by setting  $\dot{\tau} = 0$ , which lead for isentropic initial conditions for  $l = 0$  to

$$N_{0,0} = -\frac{1}{2} \Psi_0 \quad , \quad N_{0,1} = -\Phi_1 \quad \text{and} \quad N_{0,2} = -\Phi_2 - \frac{k^2}{6} \Psi_0 \quad (C.14)$$

for  $l = 1$  to

$$N_{1,1} = \frac{k}{2} \Psi_0 \quad , \quad N_{1,2} = k(\Psi_1 - \Phi_1) \quad \text{and} \quad (C.15)$$

$$N_{1,3} = k \left[ \Psi_2 - \Phi_2 - \frac{k^2}{6} \left( 1 + \frac{4}{5} K_2 \right) \Psi_0 \right]$$

and for  $l = 2$  to

$$N_{2,2} = \frac{1}{3} k^2 \sqrt{K_2} \Psi_0 \quad , \quad N_{2,3} = \frac{2}{3} k^2 \sqrt{K_2} (\Psi_1 - \Phi_1) \quad \text{and} \quad (C.16)$$

$$N_{2,4} = \frac{2}{3} k^2 \sqrt{K_2} \left[ \Psi_2 - \Phi_2 - k^2 \left\{ \frac{1}{6} + \frac{2}{15} K_2 + \frac{9}{70} K_3 \right\} \Psi_0 \right] \quad ,$$

and for  $l = 3$  to

$$N_{3,3} = \frac{1}{5} k^3 \sqrt{K_2} \sqrt{K_3} \Psi_0 \quad . \quad (C.17)$$

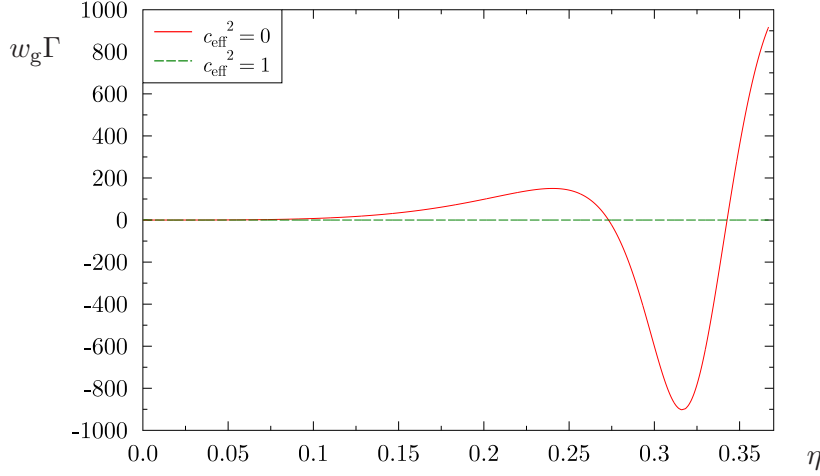


**Figure 11.** The weighted entropy perturbation  $w_g \Gamma$  of the UDM component is plotted for the two cases  $c_{\text{eff}}^2 = 0$  and  $c_{\text{eff}}^2 = 1$  for the wave number  $k = 2000$  using the best-fit model parameters.

## D Isentropic initial condition

In this appendix, it is demonstrated that the initial condition (3.2) implies a vanishing entropy perturbation  $\Gamma$  for  $\eta \rightarrow 0$ , so that the initial condition is a genuine isentropic initial condition without an isocurvature contribution. From the definition (3.6)

$$w_g \Gamma = (c_{\text{eff}}^2 - c_g^2) \delta_g^{(\text{rest})}$$

follows that one has to show  $\lim_{\eta \rightarrow 0} \delta_g^{(\text{rest})} = 0$ , if  $\lim_{\eta \rightarrow 0} (c_{\text{eff}}^2 - c_g^2)$  is finite and not necessarily equal to zero. For the UDM model discussed in this paper, one has  $\lim_{\eta \rightarrow 0} (c_{\text{eff}}^2 - c_g^2) = c_{\text{eff}}^2$  because of  $\lim_{\eta \rightarrow 0} c_g^2 = w_g(0) = w_0 = 0$  and  $0 \leq c_{\text{eff}}^2 \leq 1$ . To see the vanishing of  $\delta_g^{(\text{rest})}$ , one notes from the preceding appendices  $\delta_g = -\frac{3}{2}(1 + w_0)\Psi_0 + O(\eta)$ ,  $v_g = \frac{k}{2}\Psi_0\eta + O(\eta^2)$  and  $w_g = w_0 + O(\eta)$ , which determine the behaviour at early times of  $\delta_g^{(\text{rest})}$  given in (3.7)

$$\begin{aligned} \delta_g^{(\text{rest})} &= \delta_g + 3 \frac{\dot{a}}{a} (1 + w_g) \frac{v_g}{k} \\ &= -\frac{3}{2}(1 + w_0)\Psi_0 + 3 \frac{1}{\eta} (1 + w_0) \frac{1}{k} \frac{k}{2} \Psi_0 \eta + O(\eta) = O(\eta) \quad . \end{aligned}$$

This shows that no entropy perturbation is initially present also for  $w_0 \neq 0$ . This is confirmed in figure 11 which shows the weighted entropy perturbation  $w_g \Gamma$  for the best-fit model using the wave number  $k = 2000$ . For small values of  $\eta$  the quantity  $w_g \Gamma$  approaches zero. The significant difference between the two extreme cases  $c_{\text{eff}}^2 = 0$  and  $c_{\text{eff}}^2 = 1$  occurs at later times and is due to the fact that the energy perturbation of the unified dark matter component increases in the first case but decays in the second case. The different behaviour of the unified dark matter is visualised together with the various other components in figure 12, where the modulus of the relative energy density perturbations  $|\delta_x|$  is plotted. Note that figure 12 uses a logarithmic scaling in contrast to the linear scaling in figure 11. The energy density perturbations of the baryonic and the UDM component are almost identical at small values

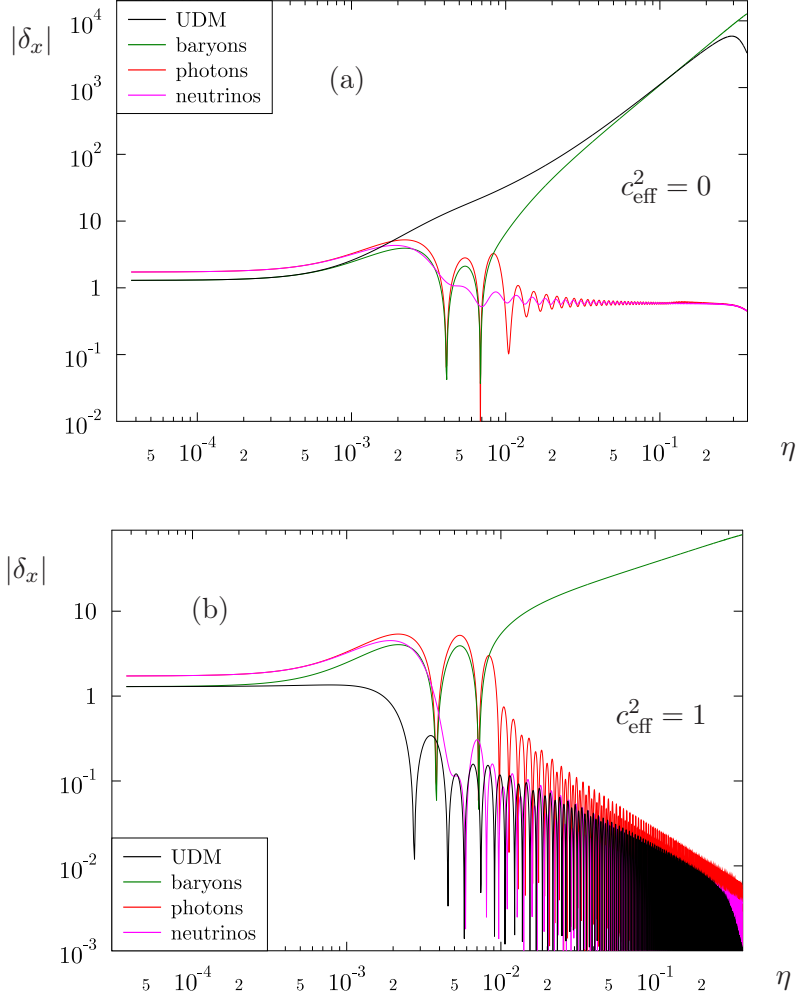


**Figure 12.** The modulus of the relative energy density perturbations  $|\delta_x|$  of the various components is plotted in dependence on conformal time  $\eta$ . The panels (a) and (b) show the results for  $c_{\text{eff}}^2 = 0$  and  $c_{\text{eff}}^2 = 1$ , respectively. The cosmological parameters are those of the best-fit model leading to a recombination time  $\eta_{\text{rec}} = 0.00745$ , and the wave number  $k = 2000$  is used.

of the conformal time  $\eta$ . The initial perturbations of the photonic and neutrino components are larger than those of the matter components due to the condition (3.2). For the case  $c_{\text{eff}}^2 = 0$ , shown in figure 12(a), the UDM energy perturbation increases and the baryonic density perturbation approaches after the recombination that of the UDM component. This leads to the large baryonic clustering necessary for the structure formation as in the usual  $\Lambda$ CDM model. The case with  $c_{\text{eff}}^2 = 1$ , shown in figure 12(b), possesses a decaying UDM energy perturbation and the baryonic energy perturbation increases only with a much lower rate after the recombination as the comparison with panel (a) reveals. This leads to the different behaviour of the entropy at late times as seen in figure 11.

## Acknowledgments

The Planck 2015 data [29] from the LAMBDA website ([lambda.gsfc.nasa.gov](http://lambda.gsfc.nasa.gov)) were used in this work.

## References

- [1] W. Hu, *Structure formation with generalized dark matter*, *Astrophys. J.* **506** (1998) 485–494, [[arXiv:astro-ph/9801234](#)].
- [2] A. Kamenshchik, U. Moschella, and V. Pasquier, *An alternative to quintessence*, *Physics Letters B* **511** (2001) 265–268, [[gr-qc/0103004](#)].
- [3] J. C. Fabris, S. V. B. Goncalves, and P. E. de Souza, *Density perturbations in an Universe dominated by the Chaplygin gas*, *Gen. Rel. Grav.* **34** (2002) 53–63, [[gr-qc/0103083](#)].
- [4] N. Bilić, G. B. Tupper, and R. D. Viollier, *Unification of dark matter and dark energy: the inhomogeneous Chaplygin gas*, *Physics Letters B* **535** (2002) 17–21, [[astro-ph/0111325](#)].
- [5] M. C. Bento, O. Bertolami, and A. A. Sen, *Generalized Chaplygin gas, accelerated expansion, and dark-energy-matter unification*, *Phys. Rev. D* **66** (2002) 043507, [[gr-qc/0202064](#)].
- [6] D. Carturan and F. Finelli, *Cosmological effects of a class of fluid dark energy models*, *Phys. Rev. D* **68** (2003) 103501, [[astro-ph/0211626](#)].
- [7] M. Makler, S. Q. de Oliveira, and I. Waga, *Constraints on the generalized Chaplygin gas from supernovae observations*, *Physics Letters B* **555** (2003) 1–6, [[astro-ph/0209486](#)].
- [8] H. B. Sandvik, M. Tegmark, M. Zaldarriaga, and I. Waga, *The end of unified dark matter?*, *Phys. Rev. D* **69** (2004) 123524, [[astro-ph/0212114](#)].
- [9] O. F. Piattella, *The extreme limit of the generalised Chaplygin gas*, *J. Cosmology and Astroparticle Physics* **3** (2010) 12, [[arXiv:0906.4430](#) [[astro-ph.CO](#)]].
- [10] R. R. Reis, I. Waga, M. O. Calvão, and S. E. Jorás, *Entropy perturbations in quartessence Chaplygin models*, *Phys. Rev. D* **68** (2003) 061302, [[astro-ph/0306004](#)].
- [11] R. J. Scherrer, *Purely Kinetic  $k$  Essence as Unified Dark Matter*, *Phys. Rev. Lett.* **93** (2004) 011301, [[astro-ph/0402316](#)].
- [12] J. K. Erickson, R. R. Caldwell, P. J. Steinhardt, C. Armendariz-Picon, and V. Mukhanov, *Measuring the Speed of Sound of Quintessence*, *Phys. Rev. Lett.* **88** (2002) 121301, [[astro-ph/0112438](#)].
- [13] S. DeDeo, R. R. Caldwell, and P. J. Steinhardt, *Effects of the sound speed of quintessence on the microwave background and large scale structure*, *Phys. Rev. D* **67** (2003) 103509, [[astro-ph/0301284](#)].
- [14] D. Bertacca, N. Bartolo, and S. Matarrese, *Unified Dark Matter Scalar Field Models*, *Advances in Astronomy* **2010** (2010) 904379, [[arXiv:1008.0614](#) [[astro-ph.CO](#)]].
- [15] W. S. Hipólito-Ricaldi, H. E. S. Velten, and W. Zimdahl, *Non-adiabatic dark fluid cosmology*, *J. Cosmology and Astroparticle Physics* **6** (2009) 16, [[arXiv:0902.4710](#) [[astro-ph.CO](#)]].
- [16] O. F. Piattella, D. Bertacca, M. Bruni, and D. Pietrobon, *Unified Dark Matter models with fast transition*, *J. Cosmology and Astroparticle Physics* **1** (2010) 14, [[arXiv:0911.2664](#) [[astro-ph.CO](#)]].
- [17] D. Bertacca, M. Bruni, O. F. Piattella, and D. Pietrobon, *Unified Dark Matter scalar field models with fast transition*, *J. Cosmology and Astroparticle Physics* **02** (2011) 018, [[arXiv:1011.6669](#) [[astro-ph.CO](#)]].

- [18] J. P. Campos, J. C. Fabris, R. Perez, O. F. Piattella, and H. Velten, *Does Chaplygin gas have salvation?*, *European Physical Journal C* **73** (2013) 2357, [[arXiv:1212.4136 \[astro-ph.CO\]](#)].
- [19] H. A. Borges, S. Carneiro, J. C. Fabris, and W. Zimdahl, *Non-adiabatic Chaplygin gas*, *Physics Letters B* **727** (2013) 37–42, [[arXiv:1306.0917 \[astro-ph.CO\]](#)].
- [20] M. Bruni, R. Lazkoz, and A. Rozas-Fernández, *Phenomenological models for unified dark matter with fast transition*, *Mon. Not. R. Astron. Soc.* **431** (2013) 2907–2916, [[arXiv:1210.1880 \[astro-ph.CO\]](#)].
- [21] T. R. P. Caramês, J. C. Fabris, and H. E. S. Velten, *Spherical collapse for unified dark matter models*, *Phys. Rev. D* **89** (2014) 083533, [[arXiv:1401.5608 \[astro-ph.CO\]](#)].
- [22] S. Kumar and A. A. Sen, *Clustering GCG: a viable option for unified dark matter-dark energy?*, *J. Cosmology and Astroparticle Physics* **10** (2014) 36, [[arXiv:1405.5688 \[astro-ph.CO\]](#)].
- [23] R. Lazkoz, I. Leanizbarrutia, and V. Salzano, *Cosmological constraints on fast transition Unified Dark Matter models*, *Journal of Physics Conference Series* **600** (2015) 012028.
- [24] R. R. Cuzinatto, L. G. Medeiros, and E. M. de Moraes, *Observational constraints to a unified cosmological model*, *Astroparticle Physics* **73** (2016) 52–61, [[arXiv:1412.0145 \[astro-ph.CO\]](#)].
- [25] C. Ma and E. Bertschinger, *Cosmological perturbation theory in the synchronous and conformal Newtonian gauges*, *Astrophys. J.* **455** (1995) 7–25.
- [26] W. Hu, *Wandering in the Background: A CMB Explorer*. PhD thesis, University of California at Berkeley, 1995. [arXiv:astro-ph/9508126](#).
- [27] V. F. Mukhanov, H. A. Feldman, and R. H. Brandenberger, *Theory of cosmological perturbations*, *Physics Report* **215** (1992) 203–333.
- [28] G. Ballesteros and J. Lesgourgues, *Dark energy with non-adiabatic sound speed: initial conditions and detectability*, *J. Cosmology and Astroparticle Physics* **10** (2010) 14, [[arXiv:1004.5509 \[astro-ph.CO\]](#)].
- [29] Planck Collaboration, R. Adam, P. A. R. Ade, N. Aghanim, Y. Akrami, M. I. R. Alves, M. Arnaud, F. Arroja, J. Aumont, C. Baccigalupi, and et al., *Planck 2015 results. I. Overview of products and scientific results*, [arXiv:1502.01582 \[astro-ph.CO\]](#).
- [30] Planck Collaboration, P. A. R. Ade, N. Aghanim, C. Armitage-Caplan, M. Arnaud, M. Ashdown, F. Atrio-Barandela, J. Aumont, C. Baccigalupi, A. J. Banday, and et al., *Planck 2013 results. XVI. Cosmological parameters*, *Astron. & Astrophys.* **571** (2014) A16, [[arXiv:1303.5076 \[astro-ph.CO\]](#)].
- [31] Planck Collaboration, P. A. R. Ade, N. Aghanim, M. Arnaud, M. Ashdown, J. Aumont, C. Baccigalupi, A. J. Banday, R. B. Barreiro, N. Bartolo, and et al., *Planck 2015 results. XIV. Dark energy and modified gravity*, [arXiv:1502.01590 \[astro-ph.CO\]](#).